J. Opt. **15** (2013) 114006 (7pp) doi:10.1088/2040-8978/15/11/114006

Soft-boundary graphene nanoribbon formed by a graphene sheet above a perturbed ground plane: conductivity profile and SPP modal current distribution

Ebrahim Forati and George W Hanson

Department of Electrical Engineering and Computer Science, University of Wisconsin Milwaukee, WI 53211, USA

E-mail: eforati@uwm.edu and george@uwm.edu

Received 30 May 2013, accepted for publication 9 July 2013
Published 28 October 2013
Online at stacks.iop.org/JOpt/15/114006

Abstract
An infinite sheet of graphene lying above a perturbed ground plane is studied. The perturbation is a two-dimensional ridge, and a bias voltage is applied between the graphene and the ground plane, resulting in a graphene nanoribbon-like structure with a soft boundary (SB). The spatial distribution of the graphene conductivity forming the SB is studied as a function of the ridge parameters and the bias voltage. The current distribution of the fundamental transverse magnetic surface plasmon polariton (SPP) is considered. The effect of the ridge parameters and shape of the SB on the current distributions are investigated, and the conditions are studied under which the mode remains confined to the vicinity of the ridge region.

Keywords: graphene nanoribbon, surface plasmon polariton, graphene conductivity

(Some figures may appear in colour only in the online journal)

1. Introduction

Graphene is a two-dimensional material having unique electronic, mechanical, and optical properties [1–6]. A variety of applications have been considered, including optical sensors [7], transparent electrodes, nanoelectromechanical applications (NEMs) [8], and optoelectronic applications [9–12]. Graphene's interesting properties are partly due to its conical conduction and valance bands joined by two points at the Fermi level [13]. Graphene, doped with excess carriers, can also guide surface plasmon oscillations at terahertz frequencies, similar to those in noble metals at infrared frequencies [14, 15]. In this regard, at THz frequencies graphene has attractive plasmonic properties, exhibiting long-lived excitations and SPP tunability. The tunability of transverse magnetic (TM) surface plasmons is due to their ability to vary the carrier density, which can be easily achieved by gate biasing or chemical doping. Graphene can also support transverse electric (TE) surface plasmons which are loosely confined to its surface; we do not consider them further in this paper. Electron energy-loss spectroscopy (EELS) was first used to prove the existence of the plasmonic effect in graphene experimentally [16, 17]. Later, surface plasmons were excited via optical means and the interaction of optical phenomena with graphene plasmons was studied experimentally [18, 19]. Considering only TM surface plasmons, an infinite suspended sheet of graphene supports one surface mode. However, a graphene strip supports an infinite number of 2D-bulk modes and two almost degenerate symmetrical and anti-symmetrical edge modes. Therefore, graphene strips are of obvious interest for waveguiding and related applications due to the variety of possible modes that may propagate. Also, plasmons in graphene with a magnetic field present have been studied [20, 21]

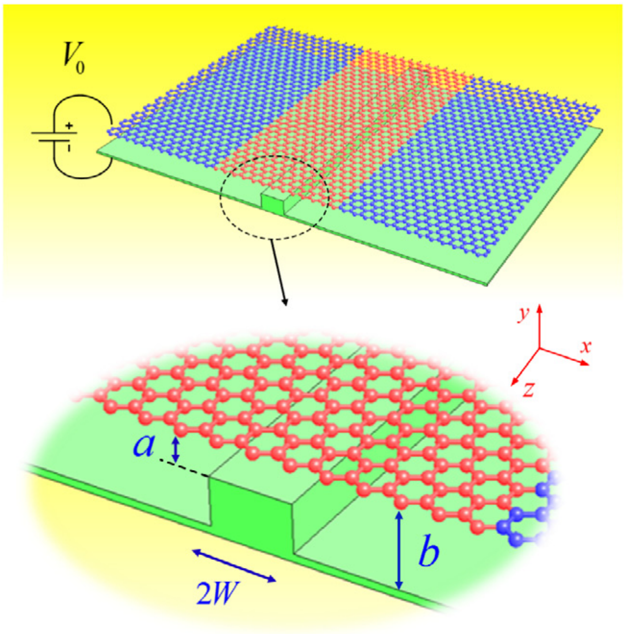

Figure 1. Electrostatically biased graphene sheet over a ground plane with a two-dimensional ridge.

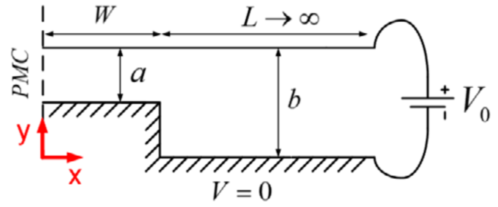

Figure 2. The x–y view of the geometry in figure 1.

and shown to have interesting properties. For example, a magnetically biased graphene strip supports edge and bulk magnetoplasmons with nonreciprocal properties.

Electrically, graphene can be modeled by surface conductivity which is considered in several works [22–30]. Here we use the local conductivity resulting from the Kubo formula [31]

$$\sigma(x) = \frac{\mathrm{j}e^2}{\pi\hbar^2(\omega - \mathrm{j}\Gamma)} \int_0^\infty \varepsilon \left(\frac{\partial f_\mathrm{d}(\varepsilon, x)}{\partial \varepsilon} - \frac{\partial f_\mathrm{d}(-\varepsilon, x)}{\partial \varepsilon} \right) \mathrm{d}\varepsilon - \frac{\mathrm{j}e^2(\omega - \mathrm{j}\Gamma)}{\pi\hbar^2} \int_0^\infty \frac{f_\mathrm{d}(-\varepsilon, x) - f_\mathrm{d}(\varepsilon, x)}{(\omega - \mathrm{j}\Gamma)^2 - 4(\varepsilon/\hbar)^2} \mathrm{d}\varepsilon, \qquad (1)$$

where $-e$ is the charge of an electron, $\hbar$ is the reduced Plank's constant, $f_\mathrm{d}(\varepsilon, x) = (\exp\left(\frac{\varepsilon - \mu_\mathrm{c}(x)}{k_\mathrm{B}T}\right) + 1)^{-1}$ is the Fermi–Dirac distribution, k_B is the Boltzmann's constant, $\mu_\mathrm{c}(x)$ is the inhomogeneous chemical potential created by the bias, and $\Gamma = 10^{13}\ \mathrm{s}^{-1}$ is the phenomenological scattering rate.

The first term in (1) is due to intraband contributions and the second term is due to interband contributions. The sign of $\mathrm{Im}(\sigma)$ is negative and positive for the intraband and interband contributions, respectively. Therefore, depending on the parameters in (1), such as frequency and temperature, one of the two contributions dominates and determines the sign of $\mathrm{Im}(\sigma)$.

It can be shown that TM surface waves can propagate only if $\mathrm{Im}(\sigma) < 0$ [24, 28]. This phenomenon is exploited in [32], where it is suggested that a graphene sheet and an inhomogeneous biasing scheme, such as that resulting from a ground plane ridge (figure 1), can be used to electronically form a conductivity profile capable of confining SPP propagation. That is, in [32] the ridge is assumed to achieve a piece-wise constant conductivity profile with $\mathrm{Im}(\sigma) < 0$ in the desired channel region $|x| < W$ and $\mathrm{Im}(\sigma) > 0$ outside of the channel, $|x| > W$, forming, essentially, a hard-boundary (HB) graphene nanoribbon (GNR). In this paper, we investigate this structure (figure 1) without the piece-wise constant conductivity assumption—the biased ridge/ground plane results in an electrostatic (bias) charge distribution $\rho(x)$ determined from Laplace's equation, which, in turn, results in the inhomogeneous chemical potential $\mu_\mathrm{c}(x)$ such that $\sigma = \sigma(x)$. This geometry permits the ability to tune $\mathrm{Im}(\sigma)$ to be negative in a limited area (in the vicinity of the ridge), forming a channel for SPP guiding, albeit forming a soft boundary (SB). In particular, it is impossible to form the HB case using the ridged ground plane, but one can approximate the HB case with a sufficiently sharp SB, as shown below.

The time convention is $\mathrm{e}^{\mathrm{j}\omega t}$ and the temperature in (1) is set to be $T = 3$ K, consistent with [32], since at lower temperature the interband contribution can dominate the intraband contribution down to lower frequencies than at room temperature. For example, at $f = 45$ THz and $\mu_\mathrm{c} = 0.05$ eV, the intraband and interband contributions at $T = 3$ K are $\sigma_\mathrm{intra} = 1.4 - \mathrm{j}41\ \mu\mathrm{S}$ and $\sigma_\mathrm{inter} = 8.9 + \mathrm{j}62\ \mu\mathrm{S}$ while at $T = 300$ K they are $\sigma_\mathrm{intra} = 1.4 - \mathrm{j}42\ \mu\mathrm{S}$ and $\sigma_\mathrm{inter} = 27 + \mathrm{j}39\ \mu\mathrm{S}$.

In the following, properties of the resulting channel are studied as a function of the parameters shown in figure 1. Then, the current distribution for the fundamental mode of the geometry is considered and the conditions are explored under which the mode will remain confined to the vicinity of the step region. One interesting result is that currents can still be concentrated to the vicinity of the ridge even when $\mathrm{Im}(\sigma)$ is negative everywhere. This requires some special conditions which are discussed toward the end of this work.

2. Methodology and formulations

Figure 2 shows the x–y view of the geometry in figure 1. A perfect magnetic conductor (PMC) sheet is placed at $x = 0$ since the geometry is symmetrical with respect to $x = 0$. By solving Laplace's equation and applying the appropriate boundary conditions, it is easy to show that the bias voltage distribution between the graphene and the ground plane is

$$\frac{V(x, y)}{V_0} = \begin{cases} 1 + \dfrac{y - b}{a} & |x| < W \\ \dfrac{y}{b} + \displaystyle\sum_{n=1}^{\infty} C_n \sin\left(\frac{n\pi}{b} y\right) \mathrm{e}^{-\frac{n\pi}{b}(|x| - W)} & |x| > W \end{cases} \qquad (2)$$

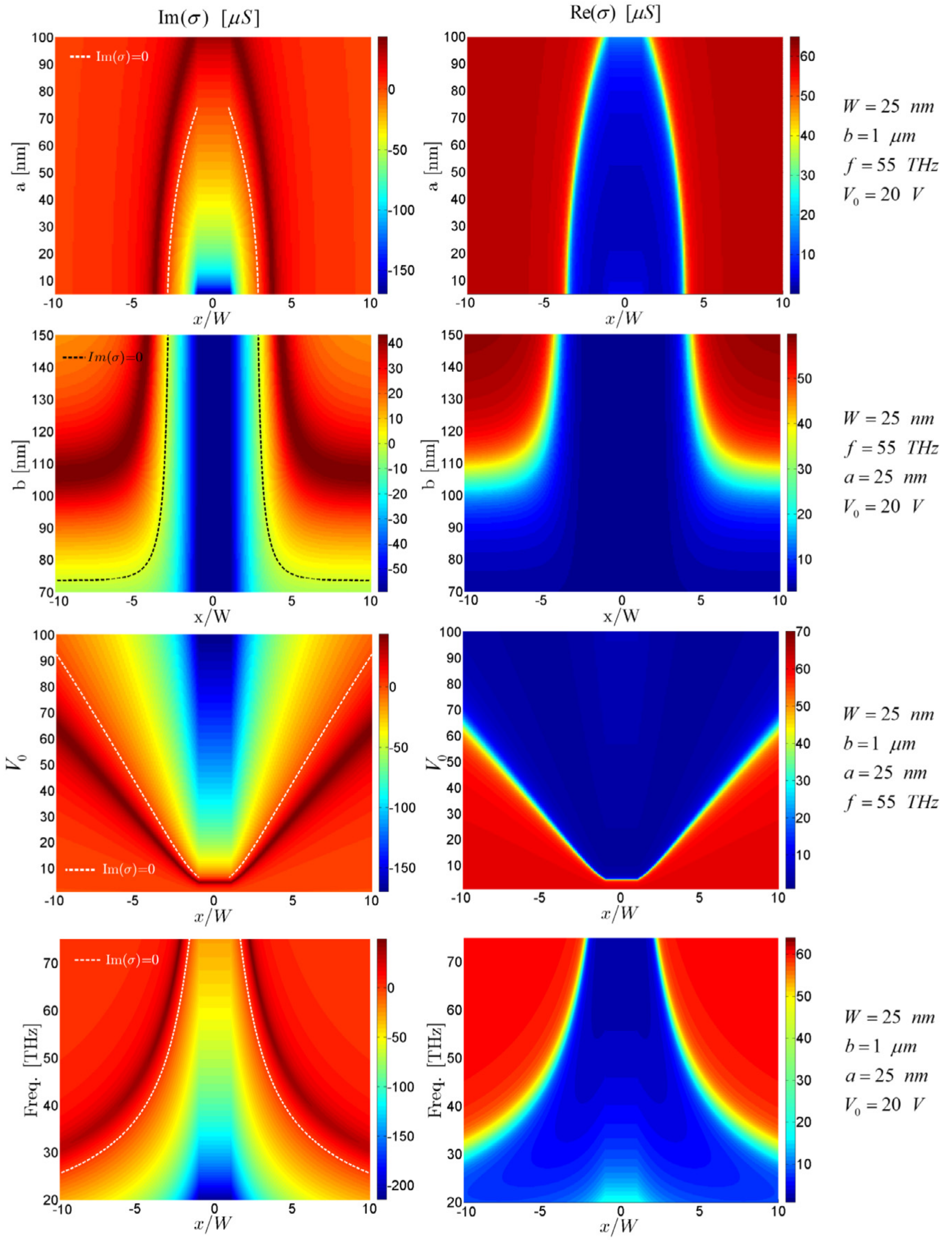

Figure 3. Imaginary (left) and real (right) parts of the conductivity distribution on the graphene sheet as a function of a, b, V_0, and frequency.

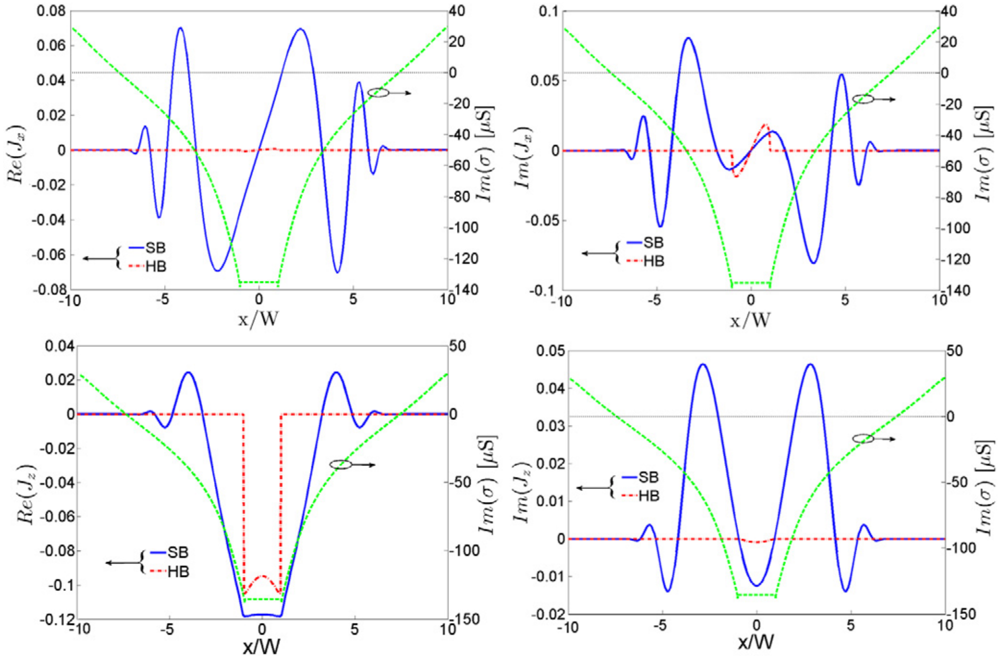

Figure 4. Longitudinal and transverse currents for the soft-boundary (blue) and the hard-boundary (red) cases, and Im(σ) profile (green). Parameters are $f = 30$ THz, $W = 25$ nm, $a = 25$ nm, $b = 1\ \mu$m, and $V_0 = 20$ V.

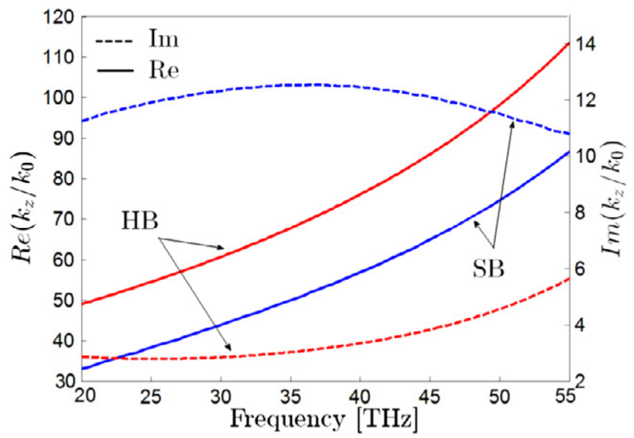

Figure 5. The dispersion curves of the fundamental mode for the soft-boundary and the hard-boundary cases. Parameters are $W = 25$ nm, $a = 25$ nm, $b = 1\ \mu$m, and $V_0 = 20$ V.

where

$$C_n = -\frac{2b}{a}\left(\frac{1}{n\pi}\right)^2 \sin\left(n\pi\left(1-\frac{a}{b}\right)\right). \tag{3}$$

In obtaining (2), a zeroth-order approximation has been used to assume an x-independent potential in the region above the step ($|x| < W$). Otherwise, the problem needs to be solved numerically (e.g., by expanding the potentials as series for both $|x| > W$ and $|x| < W$ regions). The zeroth-order solution is a good approximation for $W \ll b$ and/or $a \ll b$ in figure 1. Therefore, the electrostatic surface charge density on the graphene sheet is

$$\frac{\rho(x)}{\varepsilon_0 V_0} = \begin{cases} \dfrac{1}{a} & |x| < W \\ \dfrac{1}{b} + \displaystyle\sum_{n=1}^{\infty} \frac{n\pi}{b} C_n (-1)^n \mathrm{e}^{-\frac{n\pi}{b}(|x|-W)} & |x| > W \end{cases} \tag{4}$$

which can be used to find the chemical potential on the graphene sheet as

$$\mu_c(x) = \frac{\hbar}{e} v_F \sqrt{\frac{\pi\rho(x)}{e}} \tag{5}$$

where $v_F = 9.546 \times 10^5$ m s^{-1} is the Fermi velocity. Equation (1) then gives the conductivity distribution $\sigma(x)$ on the graphene sheet.

In order to find the dynamic modal current distributions on the graphene (eigencurrents of the structure), Ohm's law can be used in the one-dimensional Fourier transform domain $z \leftrightarrow \beta_z$ as

$$\mathbf{J}(x, \beta_z) = \sigma(x)\mathbf{E}(x, b, \beta_z), \tag{6}$$

where the Fourier transform pair is defined as

$$\mathbf{E}(x, y, \beta_z) = \int_{-\infty}^{\infty} \mathbf{E}(x, y, z)\, \mathrm{e}^{-\mathrm{j}\beta_z z}\, \mathrm{d}z \tag{7}$$

$$\mathbf{E}(x, y, z) = \frac{1}{2\pi}\int_{-\infty}^{\infty} \mathbf{E}(x, y, \beta_z)\, \mathrm{e}^{\mathrm{j}\beta_z z}\, \mathrm{d}\beta_z. \tag{8}$$

Green's theorem relates the current and the electric field as

$$\mathbf{E}(x, y, \beta_z) = \left(k_0^2 + \nabla_{\beta_z}\nabla_{\beta_z}\cdot\right) \times \int_{x'} g(x, y, x', \beta_z)\, \frac{\mathbf{J}(x', \beta_z)}{\mathrm{j}\omega\varepsilon_0}\, \mathrm{d}x' \tag{9}$$

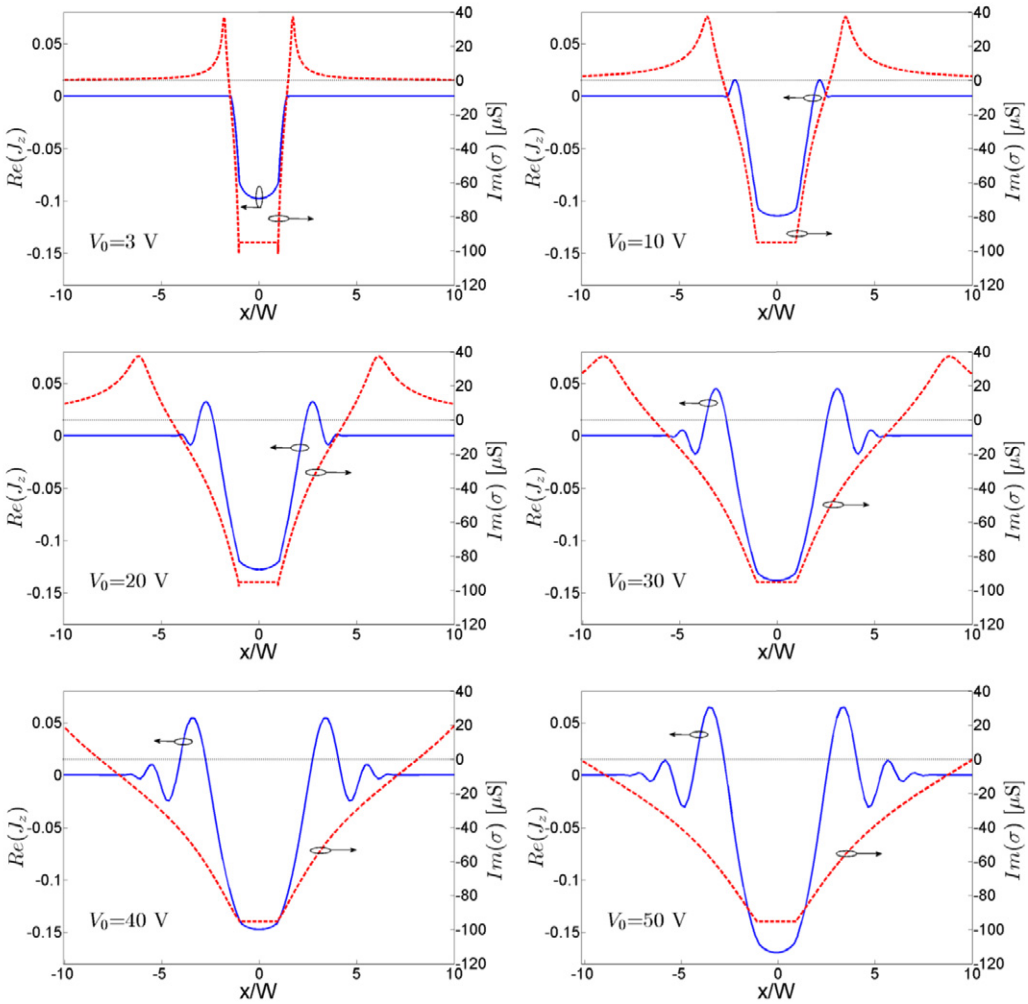

Figure 6. Real part of the longitudinal current for different values of V_0. Other parameters are $f = 40$ THz, $b = 1\ \mu$m, $W = 25$ nm, and $a = 1.25V_0$ nm.

where

$$\nabla_{\beta_z} = \frac{\mathrm{d}}{\mathrm{d}x}\hat{\mathbf{x}} + \frac{\mathrm{d}}{\mathrm{d}y}\hat{\mathbf{y}} + \mathrm{j}\beta_z\hat{\mathbf{x}}. \tag{10}$$

The Green's function in (9) is [33]

$$g\left(x, y, x', \beta_z\right) = \frac{1}{2\pi}K_0\left(\sqrt{\beta_z^2 - k_0^2}\sqrt{(x-x')^2 + (y-b)^2}\right), \tag{11}$$

where $K_0(x)$ is the zero order modified Bessel function of the first kind. Since we are considering modes tightly bound to the graphene surface, once the ridged ground plane is used to obtain the electrostatic bias charge density we assume that the ground plane does not interact with the tightly confined modal fields, which we verified to be true.

In summary, we assume the graphene sheet forms a conductive surface, we find the electrostatic potential distribution $V(x, y)$ via Laplace's equation, leading to an electrostatic charge distribution and resulting chemical potential, resulting in the conductivity $\sigma(x)$. Equations (6) and (9) form an integral equation whose null space gives the modes of the structure (i.e., different β_z and their associated currents).

The pulse function collocation method is used to solve the integral equation, with point matching at the center of the pulses. The conductivity distribution based on the electrostatic charge distribution in (6) is assumed to be only slightly perturbed by the modal fields, i.e., $\nabla \cdot \mathbf{J}/\mathrm{j}\omega \ll \rho$ where ρ is the static charge density (4) and $\mathbf{J}$ is the dynamic modal current density (6). To see that this inequality is satisfied, assume a typical frequency of $f = 30$ THz and a strip width $W = 25$ nm. If the modal current is as large as $I = |\mathbf{J}|\,2W = 1$ mA, then the left side of the inequality is 10^{-10} C m^{-2}. Using (4) with typical values $a = 25$ nm and $V_0 = 20$ V leads to $\rho = 7$ mC m^{-2} (consistent with typical doping densities of 4×10^{12} cm^{-2}), and the inequality is strongly satisfied.

3. Results and discussions

Figure 3 shows the conductivity distribution for the structure of figure 1 as a function of the ridge parameters (a and b), bias voltage, and frequency. The dashed lines in the plots for $\mathrm{Im}(\sigma)$ specify lines where $\mathrm{Im}(\sigma) = 0$, and so the distance between

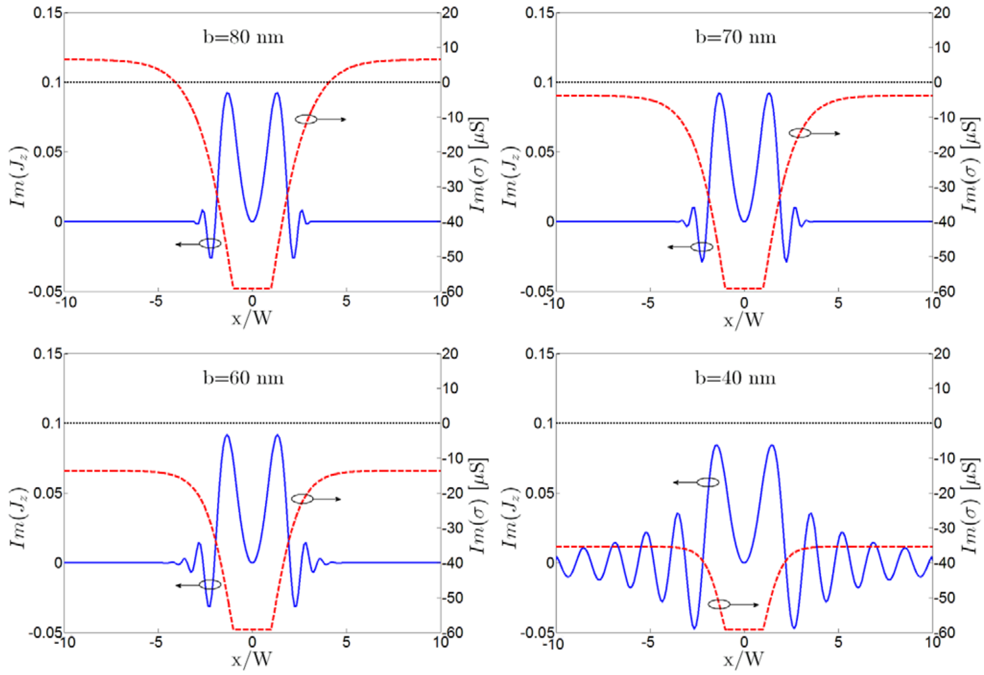

Figure 7. Imaginary part of the longitudinal current for different values of b. Other parameters are $f = 55$ THz, $V_0 = 20$ V, $W = 25$ nm, and $a = 25$ nm.

the dashed lines specifies the effective width of the channel created above the ridge with negative Im(σ). As can be seen in figure 3, the width of the channel increases by increasing the bias voltage, by decreasing a or b, or by decreasing the frequency (assuming that the other parameters are fixed in each case). The width of the channel is also more sensitive to the applied bias voltage than the other parameters. The parameter a along with the bias voltage determine the value of the conductivity in the $|x| < W$ region. The parameter b along with the bias voltage determine the value of the conductivity far away from the ridge $|x| \gg W$. However, the softness or the sharpness of the boundary is a function of all the parameters somewhat equally.

Figure 4 shows the current distribution associated with the fundamental SPP mode in figure 1. The conductivity and the current marked as SB in figure 4 correspond to the geometry in figure 1 for $f = 30$ THz, $W = 25$ nm, $a = 25$ nm, $b = 1$ μm, and $V_0 = 20$ V. The current which is noted as the HB current corresponds to a GNR having a width of 50 nm and the same conductivity as the SB case for $|x| < W$, and with $\sigma = 0$ for $|x| > W$. The dispersion curves associated with these currents are shown in figure 5. The currents in figure 4 are normalized so that the 2-norm of the eigencurrent vector (consisting of transverse and longitudinal components) is unity, $\int \left(|J_x(x)|^2 + |J_z(x)|^2\right) \mathrm{d}x = 1$. Nonetheless, only the relative current component values are important for our purposes.

As figure 4 suggests, the current distribution for $|x| < W$ is similar for both SB and HB cases (although Re (J_x) and Im (J_z) are much larger in the SB case) and they both vanish as Im(σ) becomes positive. However, the SB current has some oscillations near the two boundaries. These oscillations resemble the field oscillations in the cladding of an optical fiber with graded index cladding [34]. One of the consequences of this current spreading is that the mode becomes more lossy since parts of the current flows in the region with lower conductivity (SBs). As an example, the propagation constants for the SB and HB cases of figure 4 are $\beta_z/k_0 = 43.8 - \mathrm{j}12.3$ and $\beta_z/k_0 = 60.7 - \mathrm{j}2.8$, respectively.

Figure 6 shows the effect of the boundary softness on the current distribution (Re (J_z)) for the fundamental mode, where $f = 40$ THz, $W = 25$ nm, $b = 1$ μm, and V_0 takes different values. The parameter a is set to be $a = 1.25V_0$ nm so that the conductivity values remain the same for $|x| < W$. As figure 6 shows, the boundary becomes softer as V_0 increases and the current oscillations increase (both in magnitude and number).

In figures 4 and 6 the currents vanish as Im(σ) becomes positive, which raises the question: is it necessary for Im(σ) to be positive away from the ridge to have a confined mode? To address this question, figure 7 shows Im (J_z) and conductivity distributions for different values of b; the other parameters are $f = 55$ THz, $W = 25$ nm, $a = 25$ nm, and $V_0 = 20$ V. As figure 7 shows, Im(σ) changes sign for $b = 80$ nm, but it remains negative everywhere for $b = 70, 60$, and 40 nm. The currents remain confined to the vicinity of the ridge region even for values of b where Im(σ) remains negative everywhere. However, as b decreases the current spreads out further and the mode becomes less confined. As a result, the important factor to consider to achieve good lateral mode confinement is that the ratio of (or the difference between) Im(σ) above and away from the ridge should be large.

4. Conclusion

The conductivity and the current distributions were studied for an infinite graphene sheet over a ridge-perturbed ground plane. It was shown analytically that a channel with soft boundaries will be formed above the ridge to guide SPPs provided that the parameters are adjusted properly. It was also shown that the width of the channel is more sensitive to the bias voltage than the geometric ridge parameters. It was observed that the SPP can be kept confined to the vicinity of the ridge even if the formed channel does not have a finite width (i.e., that $\mathrm{Im}(\sigma)$ is negative everywhere) provided that the channel boundaries have sharp enough slopes. Since the width of the formed channel can be controlled by both frequency and the bias voltage, the spatial location of the current concentration (and its associated field) for a surface mode can be controlled. This can be useful in switching or frequency demultiplexing applications.

References

[1] Novoselov K S, Geim A K, Morozov S V, Jiang Y, Zhang D, Dubonos S V, Grigorieva I V and Firsov A A 2004 Electric field effect in atomically thin carbon films *Science* **306** 666–9

[2] Zhang Y, Tan Y W, Stormer H L and Kim P 2005 Experimental observation of the quantum Hall effect and Berry's phase in graphene *Nature* **438** 201–4

[3] Berger C, Song Z, Li X, Wu X, Brown N, Naud C, Mayou D, Li T, Hass J and Marchenkov A N 2006 Electronic confinement and coherence in patterned epitaxial graphene *Science* **312** 1191–6

[4] Geim A K and Novoselov K S 2007 The rise of graphene *Nature Mater.* **6** 183–91

[5] Nair R R, Blake P, Grigorenko A N, Novoselov K S, Booth T J, Stauber T, Peres N M R and Geim A K 2008 Fine structure constant defines visual transparency of graphene *Science* **320** 1308

[6] Bonaccorso F, Sun Z, Hasan T and Ferrari A C 2010 Graphene photonics and optoelectronics *Nature Photon.* **4** 611–22

[7] Schedin F, Lidorikis E, Lombardo A, Kravets V G, Geim A K, Grigorenko A N, Novoselov K S and Ferrari A C 2010 Surface-enhanced Raman spectroscopy of graphene *ACS Nano* **4** 5617–26

[8] Geim A K 2009 Graphene: status and prospects *Science* **324** 1530–4

[9] Mak K F, Sfeir M Y, Wu Y, Lui C H, Misewich J A and Heinz T F 2008 Measurement of the optical conductivity of graphene *Phys. Rev. Lett.* **101** 196405

[10] Mueller T, Xia F, Freitag M, Tsang J and Avouris P 2009 Role of contacts in graphene transistors: a scanning photocurrent study *Phys. Rev.* B **79** 245430

[11] Xia F N, Mueller T, Lin Y M, Valdes-Garcia A and Avouris P 2009 Ultrafast graphene photodetector *Nature Nanotechnol.* **4** 839–43

[12] Lee E J H, Balasubramanian K, Weitz R T, Burghard M and Kern K 2008 Contact and edge effects in graphene devices *Nature Nanotechnol.* **3** 486–90

[13] Castro Neto A H, Guinea F, Peres N M R, Novoselov K S and Geim A K 2009 The electronic properties of graphene *Rev. Mod. Phys.* **81** 109–62

[14] Christensen J, Manjavacas A, Thongrattanasiri S, Koppens F H L and de Abajo F J G 2011 Graphene plasmon waveguiding and hybridization in individual and paired nanoribbons *ACS Nano* **6** 431–40

[15] Hanson G W, Forati E, Linz W and Yakovlev A B 2012 Excitation of terahertz surface plasmons on graphene surfaces by an elementary dipole and quantum emitter: strong electrodynamic effect of dielectric support *Phys. Rev.* B **86** 235440

[16] Liu Y, Willis R F, Emtsev K V and Seyller T 2008 Plasmon dispersion and damping in electrically isolated two-dimensional charge sheets *Phys. Rev.* B **78** 201403

[17] Koch R J, Seyller T and Schaefer J A 2010 Strong phonon-plasmon coupled modes in the graphene/silicon carbide heterosystem *Phys. Rev.* B **82** 201413

[18] Ju L *et al* 2011 Graphene plasmonics for tunable terahertz metamaterials *Nature Nanotechnol.* **6** 630–4

[19] Yan H, Li X, Chandra B, Tulevski G, Wu Y, Freitag M, Zhu W, Avouris P and Xia F 2012 Tunable infrared plasmonic devices using graphene/insulator stacks *Nature Nanotechnol.* **7** 330–4

[20] Roldan R, Fuchs J-N and Goerbig M O 2009 Collective modes of doped graphene and a standard two-dimensional electron gas in a strong magnetic field: linear magnetoplasmons versus magnetoexcitons *Phys. Rev.* B **80** 085408

[21] Ferreira A, Peres N M R and Castro Neto A H 2012 Confined magneto-optical waves in graphene *Phys. Rev.* B **85** 205426

[22] Falkovsky L A and Varlamov A A 2007 Space–time dispersion of graphene conductivity *Eur. Phys. J.* B **56** 281–4

[23] Falkovsky L A and Pershoguba S S 2007 Optical far-infrared properties of a graphene monolayer and multilayer *Phys. Rev.* B **76** 153410

[24] Mikhailov S A and Ziegler K 2007 New electromagnetic mode in graphene *Phys. Rev. Lett.* **99** 016803

[25] Gusynin V P and Sharapov S G 2006 Transport of Dirac quasiparticles in graphene: Hall and optical conductivities *Phys. Rev.* B **73** 245411

[26] Gusynin V P, Sharapov S G and Carbotte J P 2006 Unusual microwave response of Dirac quasiparticles in graphene *Phys. Rev. Lett.* **96** 256802

[27] Peres N M R, Castro Neto A H and Guinea F 2006 Conductance quantization in mesoscopic graphene *Phys. Rev.* B **73** 195411

[28] Hanson G W 2008 Dyadic Green's functions and guided surface waves for a surface conductivity model of graphene *J. Appl. Phys.* **103** 064302

[29] Hanson G W 2008 Dyadic Green's functions for an anisotropic, non-local model of biased graphene *IEEE Trans. Antennas Propag.* **56** 747–57

[30] Ziegler K 2007 Minimal conductivity of graphene: nonuniversal values from the Kubo formula *Phys. Rev.* B **75** 233407

[31] Gusynin V P, Sharapov S G and Carbotte J P 2007 Magneto-optical conductivity in graphene *J. Phys.: Condens. Matter* **19** 026222

[32] Vakil A and Engheta N 2011 Transformation optics using graphene *Science* **332** 1291–4

[33] Chew W C 1995 *Waves and Fields in Inhomogeneous Media* (Piscataway, NJ: IEEE)

[34] Kong M and Shi B 2006 Field solution and characteristics of cladding modes of optical fibers *Fibre Integr. Opt.* **25** 305–21

Correction to: E. Forati and G.W. Hanson, Soft-boundary graphene nanoribbon formed by a graphene sheet above a perturbed ground plane: conductivity profile and SPP modal current distribution, J. Opt. 15, 114006 (2013).

The paper [1] had several incorrect values of graphene conductivity. The second paragraph of the second page (column 2) should read "For example, at $f = 45$ THz and $\mu_c = 0.05$ eV, the intraband and interband contributions at $T = 3$ K are $\sigma_{\text{inter}} = 60.2 + j23.3$ μS and $\sigma_{\text{intra}} = 0.73 - j20.7$ μS, while at $T = 300$ K they are $\sigma_{\text{inter}} = 50.6 + j27.5$ μS and $\sigma_{\text{intra}} = 0.84 - j23.7$ μS.

[1] E. Forati and G.W. Hanson, Soft-boundary graphene nanoribbon formed by a graphene sheet above a perturbed ground plane: conductivity profile and SPP modal current distribution, J. Opt. 15, 114006 (2013).